

A Dynamic Power Management and Dedicated Control Strategy of a Flexible Multi-Terminal HVDC Grids for Offshore Wind Farms

Asma Rekik^{*‡}, Ghada Boukettaya^{*}

^{*} Department of Electrical Engineering Bp w, University of Sfax National School of Engineering , Tunisia, 3038 Sfax

(asma.rekik@stud.enis.tn, ghada.boukettaya@enis.tn)

[‡]Corresponding Author; Asma Rekik, 3054 Sfax, Tel: +216 26 872 632,

Fax: +216 74 275 595, asma.rekik@stud.enis.tn

Received: 02.02.2021 Accepted:04.03.2021

Abstract- Renewable energy systems are becoming more and more popular on the energy market and wind power has particularly shown a great potential in the field. Many wind farms able to produce thousands of megawatts are expected to be placed offshore away from the mainland. To this end, aiming to produce a significant amount of power and achieve a high performance while being economically competitive, appropriate transmission systems ought to be designed.

This paper investigated a flexible Multi-terminal Direct current connection (MTDC), based on the voltage source converter (VSC) technology, connecting one or several offshore wind farms (OWFs) to one or different AC grids. The contribution of this article lies in the fact that it succeeded in setting up a balance between the produced power by the offshore wind farms and the received power by the different AC networks of the multi-terminal VSC-HVDC system, while checking grid constraints to prevent blackout. This was achieved by developing a global supervision system based on a dynamic power flow management and dedicated control in order to fulfil an optimisation of the modulated architecture of the studied MTDC system. The multi-terminal VSC-HVDC system was simulated using MATLAB software and the provided results show the feasibility and effectiveness of the proposed control strategy.

Keywords Offshore wind farms (OWF), multi-terminal VSC-HVDC system, balance of power, grid constraints, supervisory, control, optimization, architecture.

1. Introduction

Large-Scale offshore wind farms are drawing more and more interests owing to the future potential wind power generation. High Voltage Direct Current (HVDC) transmission systems turn out to be a very important technology for connecting these wind farms to power systems [1]. We studied the integration of the large offshore wind farms important amounts of power in the HVDC transmission system over long distances exceeding 50 km. Then, this transmitted power is connected to onshore grid points through long distance submarine cables. This interconnection was proved to be very beneficial and cost-effective compared to the conventional alternating current (AC) transmission [2]. With the various large-scale offshore wind farms in the course of preparation or in the advanced stages of programming, especially in Europe and North

America, it has become of great interest to develop technologies for an efficient and reliable connection between offshore wind farms and transmission grids, enhance better interconnections and improve the possibility of power exchange [3].

A multi-terminal direct current transmission system (MTDC) is an appropriated solution in order to provide the offshore wind farms connection and facilitate the transnational exchange with a high cost efficiency [4]. Multi-terminal HVDC-VSC systems consist of a number of converters that are connected to a common HVDC chain. Such multi-terminal DC connection enables flexible and optimum operation of wind power farms in a wide regional range [4]. The great offshore wind farms potential has pushed researchers to look for ways to insert the produced

power through this renewable source in the onshore energy in a good number of countries [5].

The electrical connection system of an offshore wind farm to a grid needs an offshore collection system and a transmission liaison to the shore. The offshore collection system gathers the produced power of the different wind turbines and imports it to a central collection point. Then, the power production of all the wind farms is transmitted to the different receptor points.

The first architecture of the offshore wind farm (OWFs) connection to a grid has been one of the most common offshore wind generation systems so far. Those offshore wind farms use AC in both of collection and transmission systems. Unfortunately, this solution was revealed to be an inadequate option for long distance connection wind farms located over 50-70 km from shore which accounts for the use of the high voltage alternating current (HVAC) transmission over these distances [6]. Reactive power compensation equipment is, therefore, required in order to improve the transmitted power quality.

In this research work, the MVAC-HVDC (a medium voltage (MV)) AC grid topology was used to interconnect the wind turbines to the offshore AC-DC converter that interconnects the produced wind power with the HVDC network. Indeed, the MVAC-HVDC enables the exploitation of the existing wind turbine technologies. This is also among the several proposed topologies that scientists are planning to use in the different future projects [3]. Certainly, the use of the DC transmission is very beneficial in order to avoid the reactive power production problem by AC cables over long offshore distance transmission [7].

Two control methods can be distinguished for the voltage control in the literature [8]. The first one is the Master-Slave control. The power balance is achieved by only one converter in this method since it uses this converter for the instantaneous control of the DC voltage. Consequently, this substation should be connected to a strong AC grid in order to adapt to such power variations. Moreover, if a failure occurs in this particular substation, it provokes a collapse of the whole DC system.

In the second method, however, many converters are used. One of these converters is applied to simultaneously control the DC voltage [4] and the others regulate the power transferred to the whole system. The voltage droop method is highly reliable and does not cause voltage oscillations. But, the disadvantage of this type of control is that it does not achieve a trade-off between power distribution and voltage fluctuations [9]. Indeed, this strategy has to work adequately in case of different communication failures. Obviously, in order to ensure a secure operation for the VSC stations, the DC voltage control should be allocated the most important role because the converters could be damaged by the DC over-voltage. On the other hand, the DC under-voltage may reduce the converter controllability [10]. If the balance of powers in the MTDC system is not guaranteed, it will cause a change of the DC voltage. Indeed, when the VSC operates as a rectifier, it injects the active power into the MTDC system; but when it operates as inverter, it extracts the active

power from the MTDC system. Thus, an increase in the DC voltage will be noticed when more active power is injected into the DC grid. Therefore, maintaining the DC voltage of the MTDC system in an allowable fixed range even in case of power variations is one of the most important challenges [11]. For the majority of papers, the droop is set at a value close to 5 %, which is the typical value for a frequency droop controller.

The OWF system integrated in the VSC-MTDC system is studied in several papers, [12][13]. The MTDC systems face many challenges such as the interaction between converters, power flow in DC lines and the control of the DC voltage. Such challenges were revealed and discussed in [14].

In this context, the use of the Voltage Droop control method is illustrated in this paper by exploiting a simple scenario and discussing the power flow through a large scale wind farm connected to a multi-terminal VSC-HVDC system. Indeed, the OWF and the different stations of the grids should respect the grid constraints to prevent the system blackout and reduce the risk of network congestion. Therefore, various rules are defined by the network manager for the different stations of the MTDC system. Thus, a new dynamic power management strategy based on bidirectional power flows and dedicated control of a flexible multi-terminal VSC-HVDC system were also developed in order to fulfil the best energy flow management with an optimised control and architecture of this system taking into account the different constraints. The optimal architecture of the modulated MTDC system was achieved either through changing the control strategy by station or through acting on the number of connected stations. Then, the system was simulated in normal and faulty cases.

The remainder of this work is organized as follows, in section2, the architecture of the studied system as well as the control of each element of the structure were presented. In section3, the overall power management strategy of the systems was discussed and the simulation results were provided in section 4. Finally the main conclusions were drawn in section 5.

2. Integration of an offshore wind Farm (OWF) into a Multi-Terminal HVDC system : Architecture and Control

2.1. The HVDC transmission concept

Among the most attractive and profitable ways to feat the OWF power is the use of the VSC-HVDC technology. Point to point VSC-HVDC connection is the most commonly used type.

Unfortunately, the power exchange between only two points; the onshore wind farm and the onshore main grid, is an important drawback in this case.

In the multi-terminal connection, this limitation does not exist since it allows the power flow between more than two points connected via mono- or bi-directional links as specified in Fig. 1.

So, the MTDC has more flexibility in its operation and works with a higher reliability. It should be safe, solid and reliable. It must also be an excellent investment in order to offer an economic return [15]. For this reason, the MTDC system control is crucial, and requires a more complex control method than the point-to-point systems case [15]. However, the impact of the intermittency nature of the wind decreases by interconnecting OWFs to other grids. Therefore, the architectural choice of an MTDC must be well developed and should involve such options as extending the number of terminals in VSC-MTDC system or changing the number of voltage droop controlled stations. This seems to be a suitable solution, but a technical and economic study is necessary to optimize the final choice.

The multi-terminal VSC-HVDCs (MTDCs) are meshed grids as presented in Fig. 1.

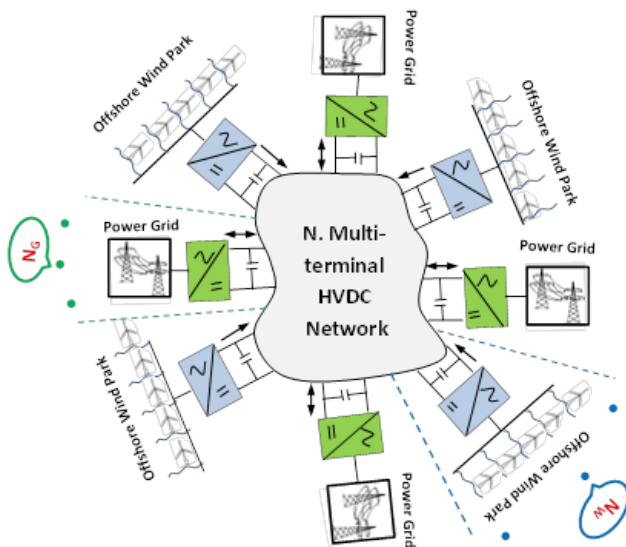


Fig. 1. Multi-Terminal HVDC system

We consider a general Multi-Terminal HVDC network coupling OWF and AC grids. We assume that this MTDC grid contains N terminal nodes (injection and consumption nodes). We define N_w as the total number of wind production nodes connected to converters which control the power transfer, N_G is the number of conventional AC grids connected to the DC grid. Some of these grids are connected to converters which control the DC voltage, while the others are connected to converters that control the power transfer. Thus, we consider that $N = N_w + N_G = N_{WP} + (N_{GVD} + N_{GP})$. Where: N_{GVD} is the number grid connected DC voltage controlled station, N_{GP} is the number of grid connected power controlled station, N_{WP} is the number of wind farms connected power controlled station.

In this paper, an OWF system connected to a four terminal voltage droop controlled HVDC system was studied. A power management algorithm was developed in order to conceive an optimal architecture based on various constraints fixed by the HVDC transmission system. This strategy would help to determine the number of converters that participate simultaneously in the regulation of the DC

voltage and the number of converters that regulate the transfer of power in the whole system. This strategy would also be generalized on an extended number of terminals.

2.2. Connection System Configuration

The most practical configurations for connecting a large OWF to an onshore station are: AC collection with AC transmission system, DC collection with DC transmission system, hybrid system and pure DC using the series converters solution [16].

The first topology MVAC/HVAC is the most commonly used type nowadays. But, the use of the HVAC transmission system is not a suitable selection for an OWF located at more than 50-70km from shore. Within such distances, it is necessary to have reactive power compensation devices in order to enhance the power quality [6].

The general structure of the second solution MVDC/HVDC is analogous to the MVAC/HVAC topology, except for the replacement of the AC cables by DC cables, and the replacement of the transformers by DC/DC converters. Since the voltage levels between different stages are not very large, this topology sounds to be a reasonable solution.

The hybrid MVAC-HVDC topology is another connection type used in many wind farm future projects [17]. In fact, the collection system in AC enables the use of the available wind turbine systems and the DC transmission is applied in order to face the problem related to the high reactive power produced by AC cables over long distance transmission. The totality of the offshore projects specified in [17] was planned to install the offshore converter substation so as to transfer the AC voltage generated by the wind farm turbines to DC, and transmit the power to the onshore side via submarine cables.

The last topology is the series parallel topology. This topology does not require a focal offshore substation. Therefore, it can be used because the offshore converter substation needs maintenance during service and requires a large initial investment in the offshore platform [18].

This paper used MVAC collection systems of the wind power production to connect the wind farms to the HVDC since it enables the use of existing wind turbine technologies. Fig.2 shows a single line diagram of VSC-HVDC system configuration with a wind AC collection system. Each permanent magnet synchronous machine (PMSG) is connected to the same DC bus via a cascaded power electronic converters. The first converter controls the PMSG (electric torque) and the second maintains the DC bus voltage between the two converters and manages the reactive (power) supplied to the distribution network. The AC output voltages of a station equipped with the wind farm turbines are stepped-up by a 50/60 Hz medium voltage transformers then assembled at a common AC coupling. Thereafter, the voltage is stepped-up again with the 50/60 Hz high voltage transformer then rectified with an AC/DC converter which is installed at the offshore platform to control the AC voltage in the collection system and transmit the produced power from this station to the other HVDC cable terminals.

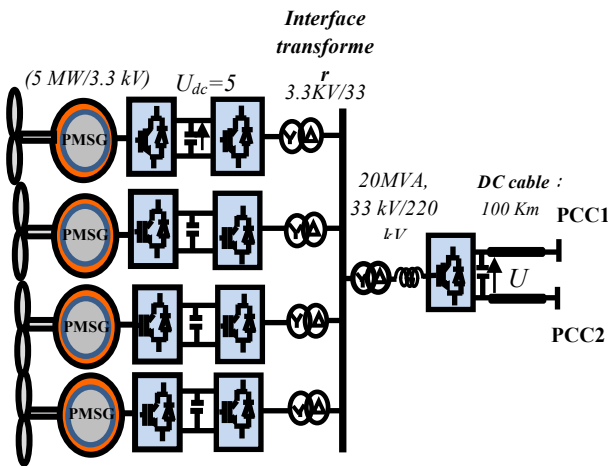


Fig. 2. Single line diagram of VSC-HVDC system configuration with AC collection system.

2.3. Integration of an OWF into four-terminal HVDC system : Topology of the studied system

The considered system consisting of the circular-network four terminal VSC-HVDC system is displayed in Fig. 3. In this figure, station 3 is an offshore wind farm that consists of

four 5 MW wind turbine and integrated in an active power controlled station. Station 4 is an onshore converter connected to the AC grid; this converter can be a power controller or an HVDC voltage droop controller. It is fixed according to the decision of the power management algorithm detailed later. Stations 1 and 2 are two onshore converters connected to two different AC grids; these converters are assigned to the HVDC voltage regulation. All the converters used in this study are Voltage Source Converters (VSCs). Indeed, the VSC-HVDC design is characterized by a more compact design occupying a smaller floor area than the line-commutated converter (LCC) based HVDC because there is no requirement for reactive power compensation. In addition, there is a risk of commutation failure in the LCC-HVDC system. However, this risk does not exist in the VSC-HVDC system owing to the use of the insulated-gate bipolar transistor (IGBT) technique [19].

The three interconnected AC grids are linked by a 50 Km long DC cable, the OWF power is about 20 MW and it is connected to the station2 and station 4 by a 100 km DC cable. All the wind power is supposed to be transferred to Stations 1, 2 and station 4.

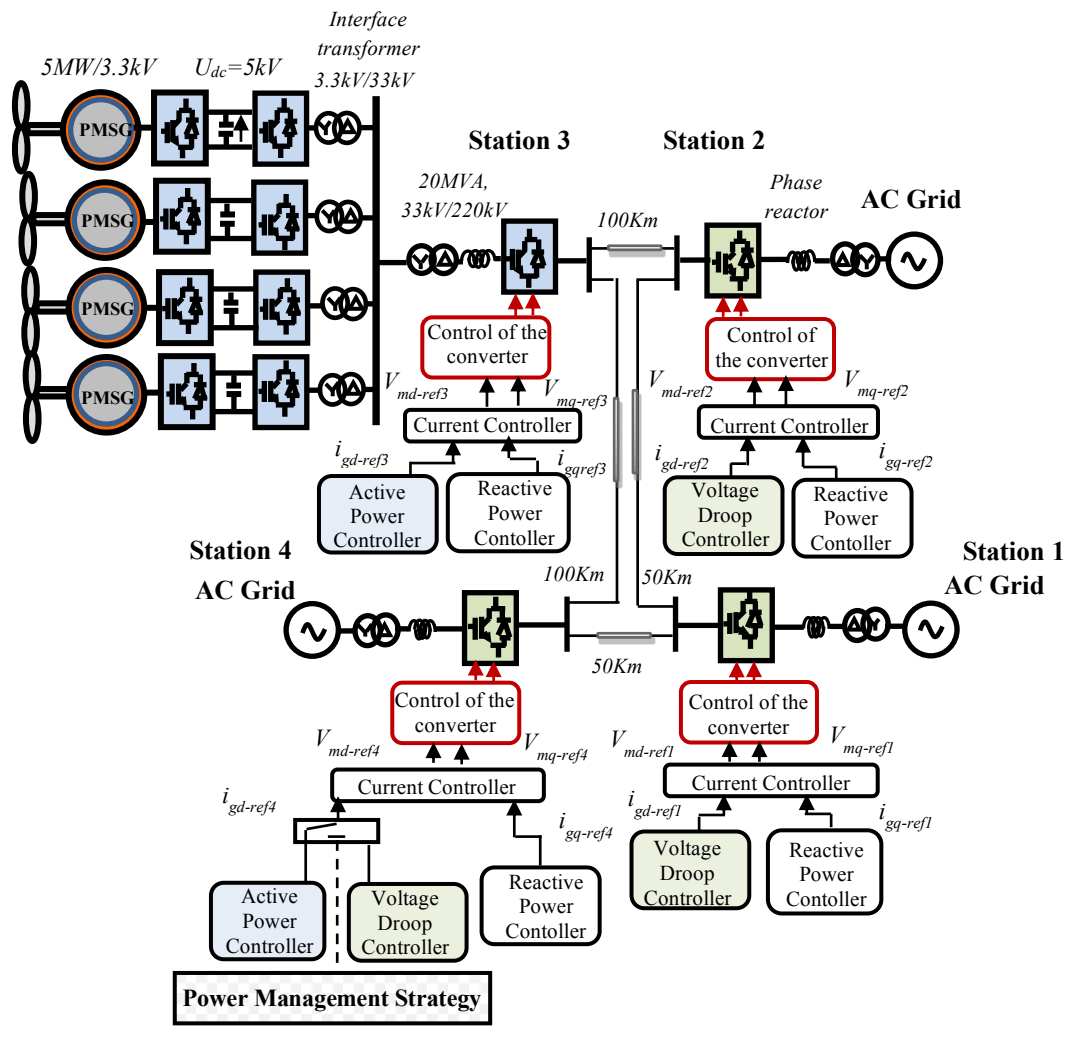


Fig. 3. A four terminal HVDC grid system.

2.4. Wind Turbine Control system structure

The coupling of a turbine with a radial magnetization with smooth poles permanent magnet synchronous generator (PMSG) and a transistor bridge rectifier [20] represents the wind generator. The model of the wind conversion system written in the Park reference frame can be expressed by the following equations:

$$\begin{pmatrix} I_{sd} \\ I_{sq} \\ \Omega \end{pmatrix} = \begin{pmatrix} -\frac{R_s}{L_s} & p\Omega & 0 \\ -p\Omega & -\frac{R_s}{L_s} & 0 \\ 0 & 0 & -\frac{f}{J} \end{pmatrix} \begin{pmatrix} I_{sd} \\ I_{sq} \\ \Omega \end{pmatrix} + \begin{pmatrix} \frac{1}{L_s} & 0 \\ 0 & \frac{1}{L_s} \end{pmatrix} \begin{pmatrix} V_{sd} \\ V_{sq} \end{pmatrix} + \begin{pmatrix} -\frac{p\Omega}{L_s} \phi_m \\ \frac{1}{J}(T_m - T_{em}) \end{pmatrix} \quad (1)$$

- (I_{sd}, I_{sq}) : Direct and quadratic components of the stator currents (A)
- (V_{sd}, V_{sq}) : Direct and quadratic components of the stator voltages (V)
- T_{em} : Electromagnetic torque (Nm)
- Ω : Rotational speed (rads⁻¹)
- p : Number of pole pairs
- ϕ_m : Permanent magnetic rotor flux (Wb)
- (R_s, L_s) : Stator winding resistance (X) and Inductance (H)
- J : Inertia (Kgm²)
- f : Friction coefficient (Nms rad⁻¹).

The wind turbine mechanical torque T_m can be expressed by:

$$T_m = \frac{1}{2} \rho \pi \frac{R^3 V^2}{\lambda} C_p(\lambda, \beta) \quad (2)$$

The power coefficient C_p depends on the pitch angle of rotor blades β and the tip s speed ratio λ with:

$$C_p(\lambda, \beta) = 0.53 \left[\frac{151}{\lambda_i} - 0.58\beta - 0.002\beta^{2.14} - 13.2 \right] \exp\left(\frac{-18.4}{\lambda_i}\right) \quad (3)$$

Where:

$$\lambda_i = \frac{1}{\frac{1}{\lambda - 0.02\beta} - \frac{0.003}{\beta^3 + 1}} \quad (4)$$

$$\lambda = \frac{R\Omega}{V_w} \quad (5)$$

V_w is the Wind Speed (ms⁻¹).

The power injected by the wind subsystem into the DC bus can be written as:

$$P_m = I_{sd} V_{sd-ref} + I_{sq} V_{sq-ref} \quad (6)$$

The dependence of the produced wind power, on control signals (V_{sd-ref}, V_{sq-ref}) which fix the power injected by the subsystem into the DC bus is indicated by the system (1).

Figure 4 shows the control structure applied to the studied PMSG wind turbine system. In fact, each of the signals (V_{sd-ref}, V_{sq-ref}) is delivered by a proportional integral regulator (PI) to respectively control the MSAP direct and quadrature current. In fact, the vector control strategy applied to the synchronous generator consists in imposing a null direct reference current (I_{sd-ref}) . The reference electromagnetic torque and the quadratic components of the stator currents (I_{sq-ref}) are proportional as given in this equation:

$$I_{sq-ref} = \frac{T_{em-ref}}{p\phi_m} \quad (7)$$

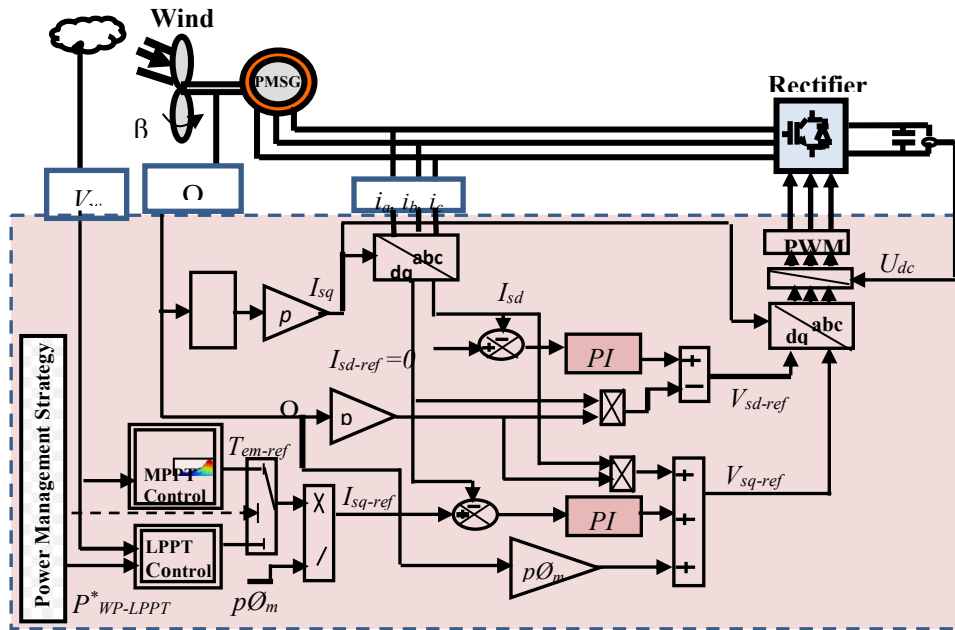


Fig. 4. Wind turbine system control structure.

The pitch angle control was implemented in three cases in this study:

- Case 1: The normal condition for the wind conversion system, while $V_w < V_{Nominal-w}$, β is fixed to zero.
- Case2: The wind speed $V_w > V_{Nominal-w}$, the rotational speed should be limited in order to inhibit the damage of the electric machine and turbine. Hence, this limitation was achieved using a closed loop control of the pitch angle β . $V_{Nominal-w} = 11.5 \text{ [ms}^{-1}\text{]}$: The minimum wind speed at which a wind turbine produces its rated power. The evolution of the pitch angle according to the speed in cases 1 and 2 is illustrated in Fig. 5.

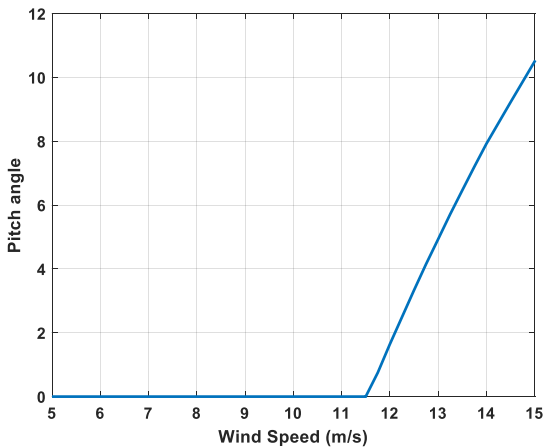
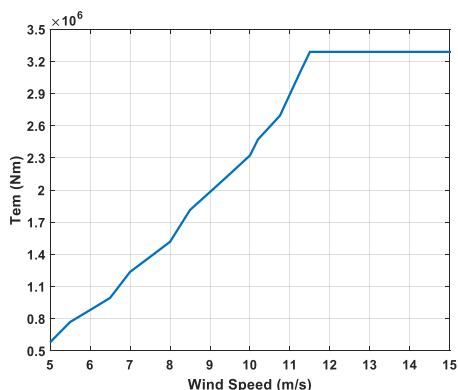


Fig. 5. Pitch angle of the wind turbine blades as function of the wind speed for maximum power point tracking (MPPT) control (cases 1 and 2).

- Case 3: This case corresponds to the limited power point tracking mode (LPPT). It was applied to efficiently manage the operation of the generation subsystems when there was a surplus of the produced wind power according to the grid code limits of each station voltage droop controlled. In fact, this mode was achieved by the implementation of a 2D look up table, already tested with two conditions:



(a) cases 1 and 2 : MPPT Mode.

The input wind $V_w(t)$ and the total reference output power $P_{WP-LPPT}^*$ of the other grids nodes of the HVDC system as given in equation (8):

$$P_{WP-LPPT}^*(t) = \sum_{j=1}^{N_{GVD}} P_{GVDj}^*(t) + P_{GP}^*(t) \quad (8)$$

Where:

- $P_{WP-LPPT}^*$: The total reference wind power limitation
- N_{GVD} : The number of voltage droop controlled stations
- P_{GVDj}^* : The reference power of j grid connected voltage droop controlled stations
- P_{GP}^* : The reference power of grid power controlled station.

The evolution of the pitch angle as function of the reference power and the wind speed in this case study is illustrated in Fig. 6.

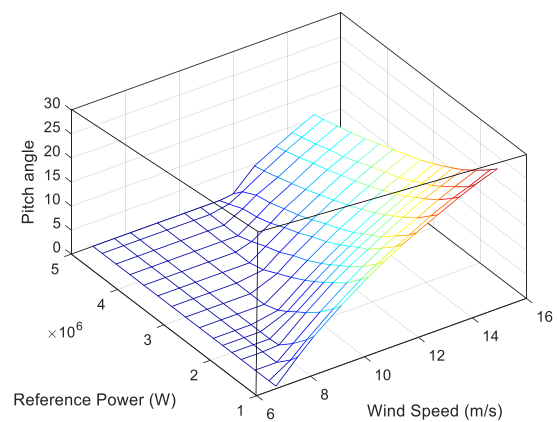
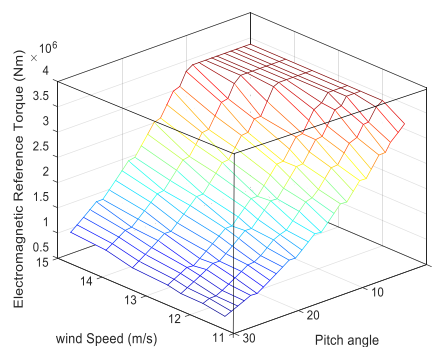


Fig. 6. The evolution of the pitch angle as function of the wind power and the reference power $\beta(V_w, P_{WP-LPPT}^*)$ for LpPt Control (Case 3).

Fig. 7 shows, respectively, the reference electromagnetic torque for the MPPT or the LPPT modes.



(b) case 3 : LpPt Mode.

Fig. 7. Reference Electromagnetic torque.

2.5. Power controller

The expressions of the active and reactive powers respectively (P, Q) in the dq frame are given by the following equation (9) :

$$\begin{cases} P = v_{gd}i_{gd} + v_{gq}i_{gq} \\ Q = v_{gq}i_{gd} - v_{gd}i_{gq} \end{cases} \quad (9)$$

The phase lock loop (PLL) has been used in order to align the voltage d -axis with the grid voltage vector; thus, system (9) can be simplified to be in the following form:

$$\begin{cases} P = v_{gd}i_{gd} \\ Q = -v_{gd}i_{gq} \end{cases} \quad (10)$$

Where :

(i_{gd}, i_{gq}): Direct and quadrature current through the phase reactor.

(V_{gd}, V_{gq}) : Direct and quadrature voltages of the AC grid.

Fig. 8 shows the active and reactive power controllers. The fundamental purpose of the power controller is to fix the active and reactive power dynamic responses.

A feed-forward action of the power controller is presented by a dotted arrow in Fig. 8 and is used in order to predict the correct control and shunt the dynamics of the power controller by instantly feeding the reference into the current controller [21].

Similarly, the power controllers guarantee that the active and reactive powers exchange at the Point of Common Coupling (PCC) and the power reference dynamics are close to those of the current loop.

Where:

(P_{ref}, Q_{ref}): The reference active and reactive power of a power controlled station, it is delivered by the grid interface transformer or wind farm interface transformer.

(i_{gd-ref}, i_{gq-ref}): Direct and quadrature current through the phase reactor.

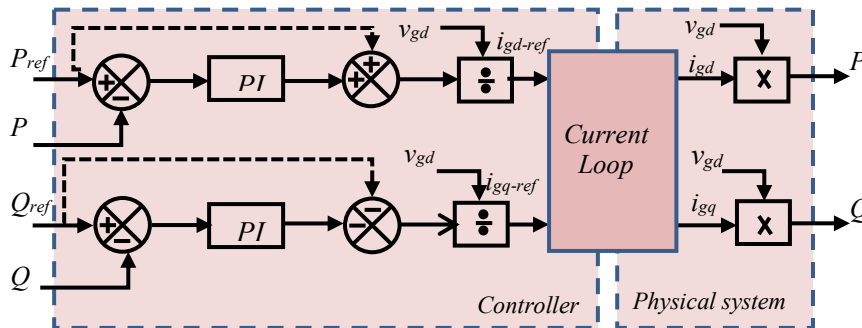


Fig. 8. Active and reactive power control loops

2.6. Design of the Current Controller

The next equations allow the expression of the AC currents using d and q coordinates of the grid voltages (V_{gd} and V_{gq}) in a $d-q$ rotating Park frame:

$$\begin{cases} \frac{di_{gd}}{dt} = \frac{1}{l_s} (v_{md} - v_{gd} - r_s i_{gd} + i_{gq} \omega l_s) \\ \frac{di_{gq}}{dt} = \frac{1}{l_s} (v_{mq} - v_{gq} - r_s i_{gq} - i_{gd} \omega l_s) \end{cases} \quad (11)$$

As shown in Fig. 9, a decoupling action and a proportional integral (PI) controller were included in the current controller; the (PI) controller was used in order to inhibit the steady state error between the reference and the output currents.

Where:

(V_{md-ref}, V_{mq-ref}) are the Direct and quadrature control voltages of converter.

(r_s, l_s) are the Resistance, Inductance of the phase reactors associated with the interface transformer filter.

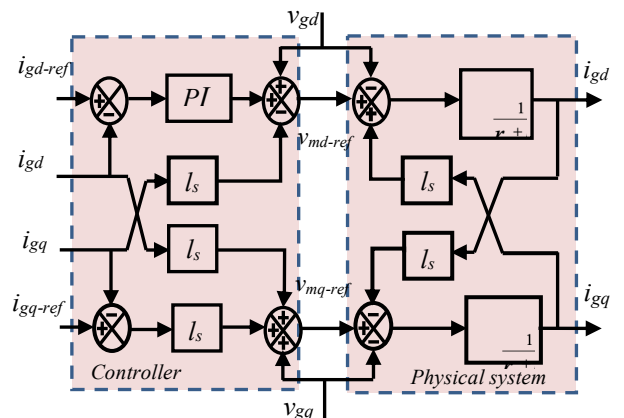


Fig. 9. Current control loops in the dq frame

2.7. Voltage Droop Control Method

Relying on the voltage Droop control method, the HVDC voltage regulation is carried out through several converters simultaneously [23]. In this subsection, the analysis of an offshore wind farm connected to the MTDC system with voltage droop control was described and applied to a four-

terminal MTDC system. To achieve the balance of power between the generation and consumption sides, a controller is necessarily used in the production units. In an AC system, the primary frequency control has been used in order to regulate the output power related with the frequency by taking a power frequency characteristic called droop control [6]. Indeed, the same principle is assumed to have a relationship between power and voltage in the power converters in DC systems. The power flow in the multi-terminal VSC-HVDC system can be controlled by a voltage droop coefficient as expressed by equation (13) [22]. The proposed method to control the studied system is illustrated in Fig. 10. Where a (PI) regulator was added to control the variation of the power injected in the DC side. Then, the output reference current i_{gd-ref} would be injected in the current controller.

$$\Delta P_g = \frac{1}{K} \Delta U_s \quad (12)$$

Where:

K is the droop value

ΔP_g is the deviation of power injected into the AC grid

ΔU_s is the deviation of DC voltage

P_{DC} is the power injected into the DC side

P_{DC-ref} is the power reference injected into the DC side.

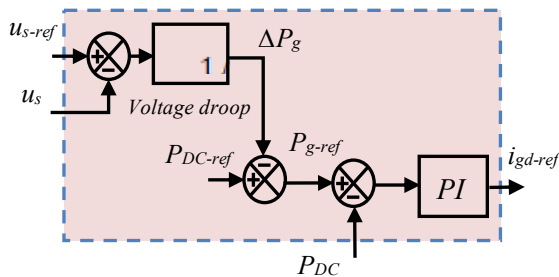


Fig. 10. Voltage droop controller

3. Power flow management strategy and dedicated control strategy

To ensure an optimal management of the energy flow distribution between the different nodes of the multi-terminal HVDC system depending on the constraints of each station during an abrupt load demand, a power management strategy was proposed. Indeed, this strategy was applied to choose the best architecture of the multi-terminal voltage droop controlled HVDC system in order to respect the interconnection grid code limitation of each station.

The different objectives ensured by the power flow management and dedicated control algorithm are:

- Choosing an appropriate droop value k that guarantees that the DC grid voltage remains within the $\pm 5\%$ bounds.
- Ensuring a balance between the generated and the consumed powers taking into account the atmospheric

conditions and the network constraints imposed by each grid code:

$$P_{WP}(t) = \sum_{j=1}^{N_{GVD}} P_{GVDj}(t) + P_{GP}(t) \quad (13)$$

Where :

P_{WP} is the power generated by the OWFs.

N_{GVD} is the number of grid connected voltage droop controlled stations.

P_{GVDj} : The power of j grid connected voltage droop controlled station.

P_{GP} : The power of grid connected power controlled station.

The powers grids receptions of each voltage droop controlled station should not exceed the limits fixed by their grid code restrictions ($P_{GVD,max}$) and the grid-generated power of each voltage droop controlled station should not exceed the limits fixed by their grid code restrictions ($P_{GVD,min}$).

- Optimizing the management strategy within the power limitations mode: If one of the MTDC stations exceeds the limitation of the generated power fixed by its grid code, two solutions can be applied according to an optimisation criterion: Either the control structure is changed from a power controlled station to a voltage droop controlled station, or the interconnection is extended by adding a new grid connected voltage droop controlled station.

- Generalizing the power management strategy for an MTDC equipped by N stations.

Fig. 11 shows the power flow management and dedicated control algorithm. The adopted algorithm requires knowledge of the initial values of the following:

- N_i , which is the number of stations of the MTDC system
- N_{GVDi} , the number of grid connected voltage droop controlled stations
- N_{GPIi} , the number of grid connected power controlled station
- K_i , the initial voltage droop coefficient
- ΔK , the decrementing value of the voltage droop coefficient
- The limits fixed by the grid code restrictions of the grid connected voltage droop controlled stations 1 and 2.
- $P_{GP}(t)$, the instantaneous value of the grid connected power controlled station
- $P_{WP-Nominal}$ the nominal value of the wind farm power.

The outputs of the algorithm are the final value of the droop coefficient K_f , the total number of stations N , the number of grid connected voltage droop controlled stations N_{GVD} , the number of the grid connected power controlled stations N_{GPI} , the reference value of the power of the each voltage droop controlled station P_{GVD}^* , the power reference value of the wind farm connected power controlled station P_{WP}^* and the reference power of the grid connected power controlled station P_{GP}^* .

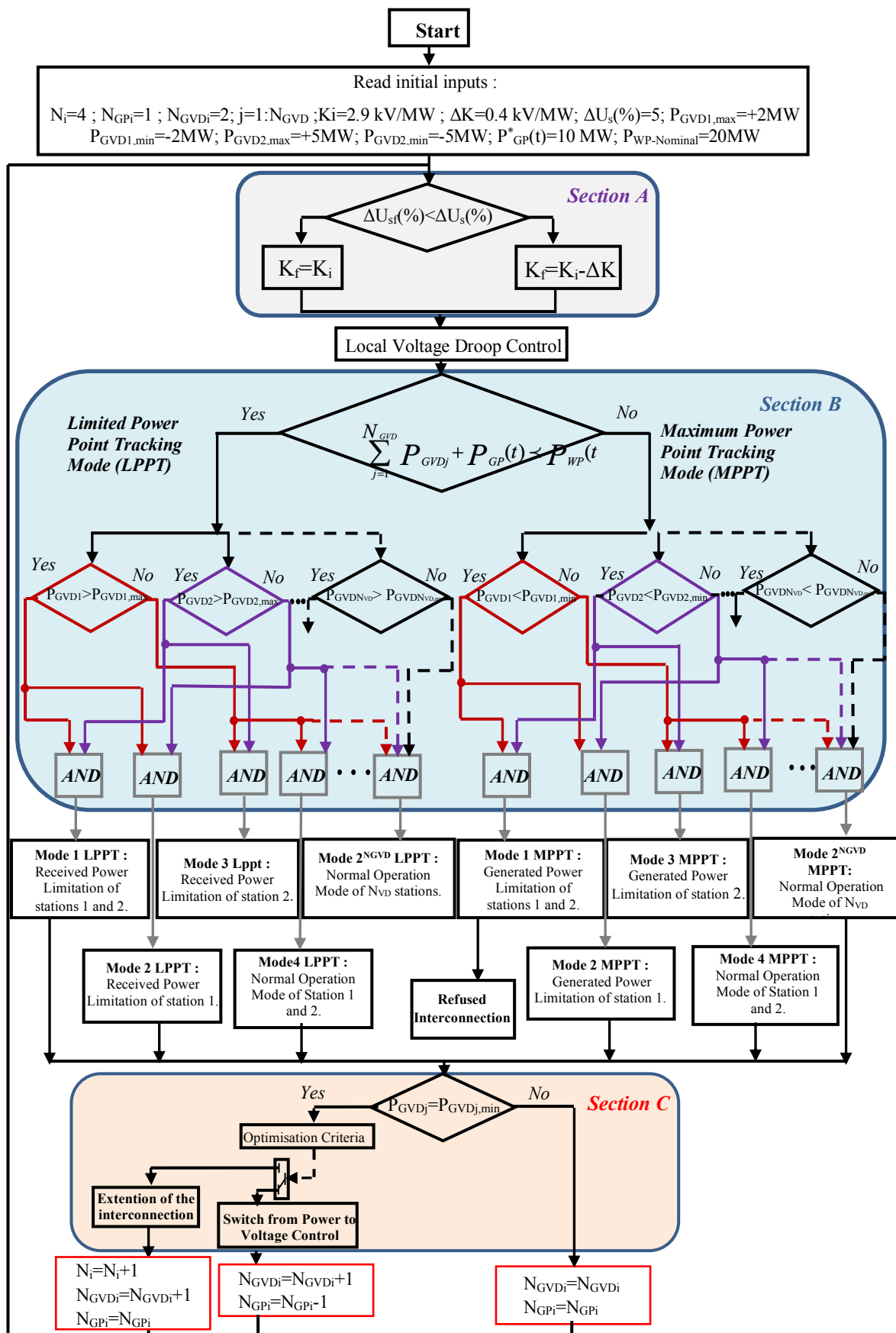


Fig. 11. Power flow management and dedicated control algorithm.

This algorithm consists of three sections A, B and C:

Section A: It represents the first control step where we choose the final droop Coefficient K_f appropriated to the deviation of the DC voltages which are given by the following equation:

$$\Delta U_s (\%) = \frac{U_{s-ref} - U_s}{U_{s-ref}} \times 100 \quad (14)$$

In fact, for an initial droop coefficient value K_i it compare the deviation of the DC voltage measured with a percentage $\Delta U_s = \pm 5\%$.

- If $\Delta U_{sf} (\%) < \Delta U_s (\%)$. The final droop coefficient K_f is set at the initially-chosen value, so $K_i = K_f$.

- If $\Delta U_{sf} (\%) > \Delta U_s (\%)$.: In order to minimize this deviation, the final droop value is decreased by a marge of ΔK which is initiated in the beginning.

Where: ΔU_{sf} : The final DC voltage deviation.

Section B: It represents a power flow management under a grid code requirement checking: The power management system algorithm serves to test both power generation and requirement to ensure the balance between the produced and consumed powers by switching between the LPPT and MPPT control of the wind farm generation system. In each control, we distinguish 2^{NGVD} LPPT or 2^{NGVD} MPPT modes.

▪ For the LPPT Control: The wind farm power generated is higher than the needed:

$$\sum_{j=1}^{N_{GVD}} P_{GVD_j} + P_{GP}(t) < P_{WP}(t) \quad (15)$$

So, a limitation of the generated wind farms power using the LPPT is required in order to satisfy the balance between the received and generated powers in accordance with the grid code restrictions. Thus, the general form of the wind farm power limitation is given by equation (16):

$$P_{WP-LPPT}^*(t) = \sum_{j=1}^{N_{GVD}} P_{GVD_j}^*(t) + P_{GP}^*(t) \quad (16)$$

Our algorithm includes the following LPPT modes:

- Mode1-LPPT: The power grid reception of voltage controlled stations 1 and 2 exceeds the limits fixed by their grid code restrictions: " $P_{GVD1} > P_{GVD1,max}$ " and " $P_{GVD2} > P_{GVD2,max}$ ", therefore, a limitation of the received power at the maximum value is required. So, in this case we use the below equation:

$$\begin{cases} P_{GVD1}^*(t) = P_{GVD1,max}(t) \\ P_{GVD2}^*(t) = P_{GVD1,max}(t) \\ P_{GP}^*(t) = P_{GP}(t) \end{cases} \quad (17)$$

- Mode2-LPPT: The power grid reception of voltage controlled station1 exceeds the limits fixed by its grid code restrictions: " $P_{GVD1} > P_{GVD1,max}$ ". So, a limitation of the received power to the maximum value is required using the following form:

$$\begin{cases} P_{GVD1}^*(t) = P_{GVD1,max}(t) \\ P_{GVD2}^*(t) = P_{GVD2}(t) \\ P_{GP}^*(t) = P_{GP}(t) \end{cases} \quad (18)$$

- Mode3-LPPT: The power grid reception of voltage controlled station2 exceeds the limits fixed by its grid code restrictions: " $P_{GVD2} > P_{GVD2,max}$ ", so, a limitation of the received power to the maximum value is required using:

$$\begin{cases} P_{GVD1}^*(t) = P_{GVD1}(t) \\ P_{GVD2}^*(t) = P_{GVD2,max}(t) \\ P_{GP}^*(t) = P_{GP}(t) \end{cases} \quad (19)$$

- Mode4-LPPT: When all the constraints fixed by the grid code restrictions are verified, we have a normal operation mode;

$$\begin{cases} P_{GVD1}^*(t) = P_{GVD1}(t) \\ P_{GVD2}^*(t) = P_{GVD2}(t) \\ P_{GP}^*(t) = P_{GP}(t) \end{cases} \quad (20)$$

- Mode $2^{N_{GVD}}$ -LPPT: This mode is referred to when we have N_{GVD} voltage droop controlled stations and all the constraints fixed by the grid code restrictions are verified. In this case, we have a generalisation of the normal operation mode:

$$\begin{cases} P_{GVD1}^*(t) = P_{GVD1}(t) \\ P_{GVD2}^*(t) = P_{GVD2}(t) \\ \bullet \\ \bullet \\ P_{GVDN_{GVD}}^*(t) = P_{GVDN_{GVD}}(t) \\ P_{GP}^*(t) = P_{GP}(t) \end{cases} \quad (21)$$

▪ For the MPPT control: This type of control is adopted when the generated wind power is less than or equal to the required amount:

$$\sum_{j=1}^{N_{GVD}} P_{GVD_j}(t) + P_{GP}(t) \geq P_{WP}(t) \quad (22)$$

So, the power of the grid connected power controlled station is limited in order to set a balance between the generated and received power in the MTDC system: Thus, the general form of the power limitation at this controlled station is given by equation (23):

$$P_{GP}^*(t) = P_{WP-MPPT}^*(t) - \sum_{j=1}^{N_{GVD}} P_{GVD_j}^*(t) \quad (23)$$

Our algorithm includes the following MPPT modes:

- Mode1-MPPT: The powers grids generation of the voltage controlled station1 and 2 exceed the limits fixed by their grid code restrictions: " $P_{GVD1} < P_{GVD1,min}$ " and " $P_{GVD2} < P_{GVD2,min}$ ". In order not to damage the MTDC system, the interconnection mode will be a refused.

- Mode2-MPPT: The power grid generation of the voltage controlled station1 exceeds the limits fixed by its grid code restrictions: " $P_{GVD1} < P_{GVD1,min}$ ". So, the power generated by station1 will be limited.

$$\begin{cases} P_{GVD1}^*(t) = P_{GVD1,min} \\ P_{GVD2}^*(t) = P_{GVD2}(t) \\ P_{WP-MPPT}^*(t) = P_{WP}(t) \end{cases} \quad (24)$$

- Mode3-MPPT: The power grid generation of the voltage controlled station 2 exceeds the limits fixed by its grid code restrictions: " $P_{GVD2} < P_{GVD2,min}$ ". So, the generated power by station2 will be limited.

$$\begin{cases} P_{GVD1}^*(t) = P_{GVD1}(t) \\ P_{GVD2}^*(t) = P_{GVD2,min} \\ P_{WP-MPPT}^*(t) = P_{WP}(t) \end{cases} \quad (25)$$

- Mode4-MPPT: All the constraints fixed by the grid code restrictions are verified, we have a normal operation mode:

$$\begin{cases} P_{GVD1}^*(t) = P_{GVD1}(t) \\ P_{GVD2}^*(t) = P_{GVD2}(t) \\ P_{WP-MPPT}^*(t) = P_{WP}(t) \end{cases} \quad (26)$$

- Mode $2^{N_{GVD}}$ -MPPT: When we have N_{GVD} grid connected voltage droop controlled stations and all the constraints fixed by the grid code restrictions are verified we generalize the normal operation mode:

$$\begin{cases} P_{GVD1}^*(t) = P_{GVD1}(t) \\ P_{GVD2}^*(t) = P_{GVD2}(t) \\ \bullet \\ \bullet \\ P_{GVDN_{GVD}}^*(t) = P_{GVDN_{GVD}}(t) \\ P_{WP-MPPT}^*(t) = P_{WP}(t) \end{cases} \quad (27)$$

Section C: This section represents the final step where the MTDC architectural configuration is achieved: The optimisation architecture of the studied MTDC system based on power flow management and dedicated control enables us to test the grid code requirements and deduce the proper architecture of the system:

If one of the MTDC stations exceeds the limitation of the generated power fixed by its grid code " $P_{GVDj} = P_{GVDj,min}$ ", where j is the number of grid connected voltage droop controlled stations varying from 1 to N_{GVD} , two solutions can be adopted depending on some optimisation criteria.

Fig. 13 shows that the choice of the droop coefficient value influences the voltage deviation which was previously defined by equation (14).

In fact, the optimization criterion is an optimal function used to adopt the appropriate mode at a lower cost [24], a maximum production of the renewable energy or in order to minimize the non-satisfaction time, based on load priority order and electricity rates.

- The first solution is to switch from a power controlled station to a voltage controlled one; so the number of grid connected voltage droop controlled stations will increase and the number of grid connected power controlled stations will decrease :

$$\begin{cases} N_{GVDi} = N_{GVDi} + 1 \\ N_{GPi} = N_{GPi} - 1 \end{cases} \quad (28)$$

- The second solution is to extend the interconnection by adding a new grid voltage droop controlled station. So we obtain:

$$\begin{cases} N_i = N_i + 1 \\ N_{GVDi} = N_{GVDi} + 1 \\ N_{GPi} = N_{GPi} \end{cases} \quad (29)$$

If no MTDC station exceeds the limitation of the generated power fixed by its grid code, there is no change in the initial MTDC system architecture.

4. Simulation Results

To prove the proposed strategy effectiveness, the simulation findings were tested for each section of the algorithm. Our case study considered a 20 MW wind farm composed of four 5MW wind turbines placed at 100 Km away from the onshore stations as shown in Fig. 3. The permanent magnet synchronous machine has a medium voltage of 3.3 kV; the DC bus at the output of the converter connected to the machine is 5 kV and the voltage of the HVDC link is 300 kV.

4.1. Validation of section A of the Power flow management and dedicated control algorithm

In order to show the influence of the droop coefficient choice on the DC voltage deviation, we used the wind speed profile displayed in Fig. 12.

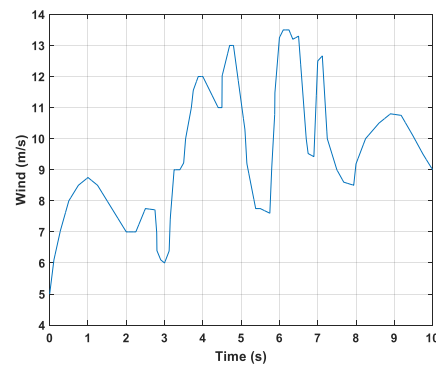


Fig. 12. First tested wind Speed profile.

The higher the droop coefficient k is, the higher the voltage deviation will be until exceeding 5 % deviation

especially when the OWFs face large disturbances in the wind farm speed input.

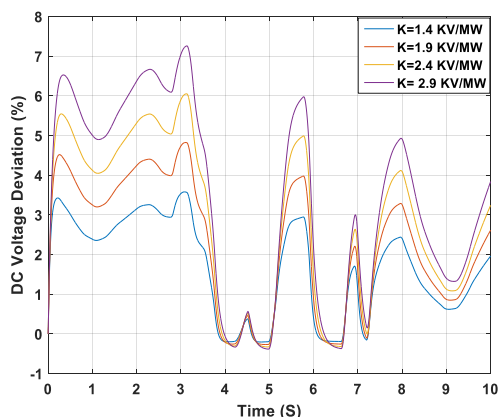


Fig. 13. DC Voltage Deviation

This section dealt with the design of the droop value. The DC voltage deviation must remain within specific bounds, and should always be set at a value close to 5 % (i.e. typical value for frequency droop controllers). According to Fig. 13 and the previously defined section A of the developed algorithm of Fig. 11, the droop value was fixed at $K=1.9$ kV/MW. In fact, the value of the droop coefficient also affects the system dynamics. The higher the droop coefficient is, the higher the DC voltage response time will be.

So, a compromise must be established between the permitted error and the system dynamics. Figs. 14 and 14a illustrate well this point.

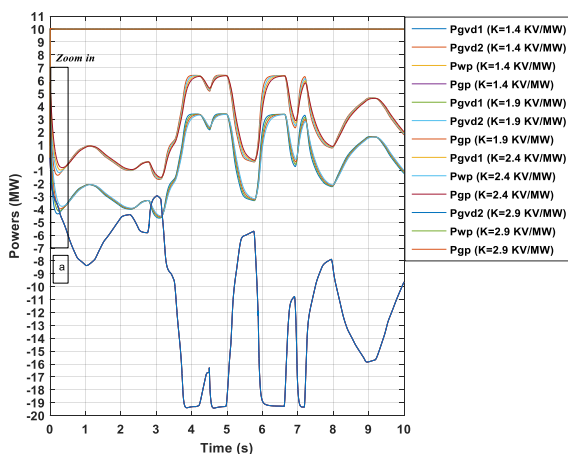


Fig. 14. Power through the four terminal HVDC converters as function of the droop coefficient.

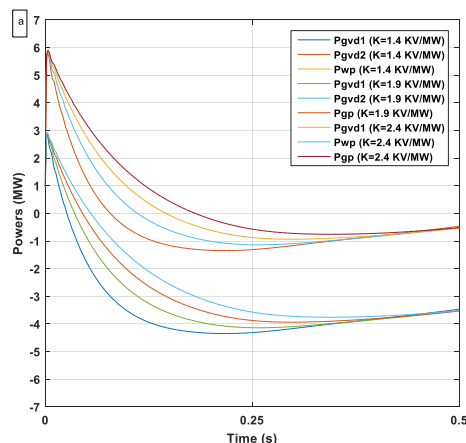


Fig 14. a. A zoomed portion of Power through the four terminal HVDC converters as function of the droop coefficient.

4.2. Optimised architecture of the MTDC system based on the power flow management and dedicated control

4.2.1. Section B validation

In order to validate section B of the power flow management and the dedicated control applied to the MTDC system, a simulation of the four terminal HVDC system was performed using < Matlab Simulink >, with the value of a droop coefficient chosen in the previous subsection ($K=1.9$ kV/MW), using a variable wind speed profile defined in Fig.12. This MTDC system consists of 2 grid connected voltage droop controlled stations, one grid connected power controlled station and one station OWF generating 20 MW. In the four terminal HVDC system, the wind farm has priority to satisfy load demands, the grid connected power controlled station is fixed as the receptive station, while the power exchange through both voltage droop controlled stations 1 and 2 is bidirectional and should respect the grid code restrictions.

Fig. 15 shows the operating mode periods of the MTDC system and validates the good functioning of section B of the supervision strategy. Fig. 16 shows the power evolution in the four terminal HVDC system with and without the developed supervision and control strategy.

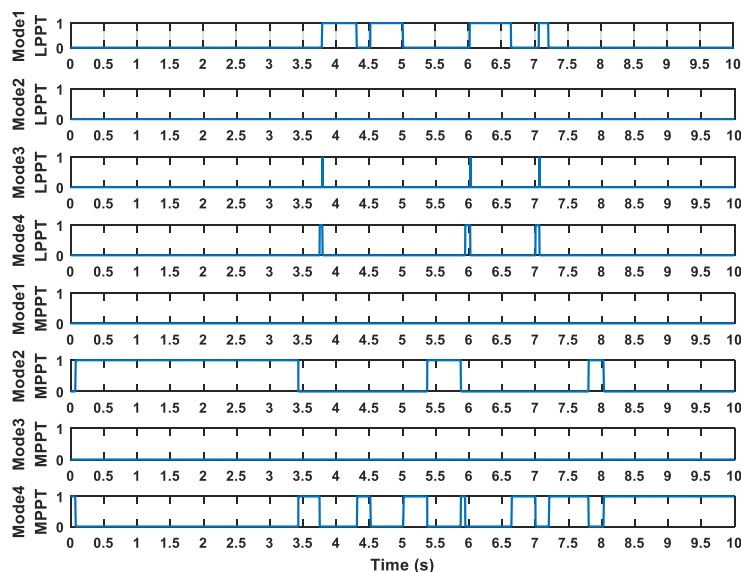


Fig. 15. Operating mode periods.

In the interval $[0, 3.4s]$ the MTDC system operates in mode 2 MPPT: generated power limitation of station 1. Indeed, the generated wind farm power is less than the required amount and the grid power generation of voltage controlled station1 exceeds the limits fixed by the grid code restrictions. So a limitation of the power generated by station1 will be imposed as illustrated in Fig. 16. (a). Besides, a limitation of the grid connected power controlled station will be carried out in order to set a balance between the generated power and the received one in the MTDC system as shown in Fig. 16. (d). This is also true for other intervals like $[5.4, 5.8s]$ and $[7.75, 8s]$.

In the period $[3.4, 3.7s]$, the MTDC system operates in mode 4 MPPT: This is the normal operation mode of the voltage droop controlled stations 1 and 2 : This mode is launched when the generated wind farm power satisfies the grid demand and all the constraints fixed by the grid code restrictions are checked as illustrated by Fig. 16 (a) and (b). The same result was achieved for the following period $[4.3, 4.5s]$, $[5, 5.4s]$, $[5.8, 5.9s]$, $[6.6, 7s]$, $[7.2, 7.75s]$ and $[8, 10s]$.

In the time intervals $[3.8, 4.3s]$ $[4.5, 5s]$ $[6.02, 6.6s]$, $[7.05, 7.2s]$, the generated wind farm power is higher than the required amount and the grid power reception of the voltage controlled stations 1 and 2 exceeds the limits fixed by their grid code. So, a limitation of the received powers at the maximum value will be imposed as shown in Fig. 16 (a) and (b). In addition, a limitation of the wind farm generated power using the LPPT will be required as given in Fig. 16 (c), in order to set a balance between the received and generated power respecting the grid code restrictions: This is mode 1 LPPT.

During the time intervals $[3.7, 3.75s]$ $[5.9, 6s]$ and $[7, 7.04s]$, the generated wind farm power is higher than the required amounts and all the constraints fixed by the grid code restrictions are checked. Therefore, in order to set the balance between the generated and received power in the

MTDC system, a limitation of the generated wind farm power will be achieved by the LPPT as shown in Fig. 16 (a), (b) and (c). It is a normal operating mode: mode 4 LPPT.

In the short time intervals $[3.75, 3.8s]$ $[6, 6.02s]$ and $[7.04, 7.05s]$ and according to mode3 LPPT, the generated wind farm power is still higher than the required amounts and only the grid power reception of station2 exceeds the grid code restriction limits; therefore, a limitation of the received power at station 2 at the maximum value will be applied as illustrated in Fig. 16 (b). Moreover, according to Fig. 16 (c), a limitation of the generated wind farm power will be carried out by the LPPT in order to set a balance between the received and generated power according to the grid restrictions code.

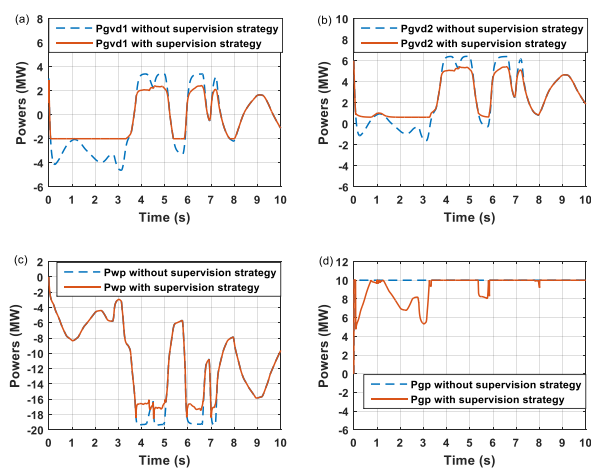


Fig 16. The power evolution in the four terminal HVDC converters with and without a supervision strategy (Section B).

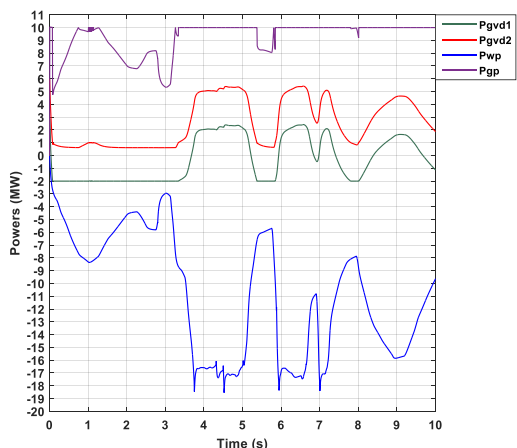


Fig. 17. Power through the four terminal HVDC converters with the supervision strategy (Section B).

Fig. 17 validates the performance of the supervision strategy to satisfy the balance between the received and generated power according to the grids limitations code.

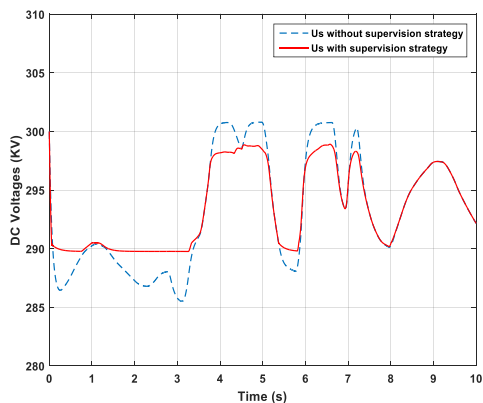


Fig. 18. DC Voltages waveform.

Fig. 18 allows us to deduce that after applying the supervision algorithm, the deviation value of the DC voltage of the MTDC system is still less than 5 % at all time period intervals, which validates section A of the supervision strategy and proves the efficiency of the algorithm.

4.2.2. Section C validation

In order to explain and validate the procedure of switching from section B to section C of the power flow management and dedicated control strategy, we used the wind speed profile displayed in Fig. 19.

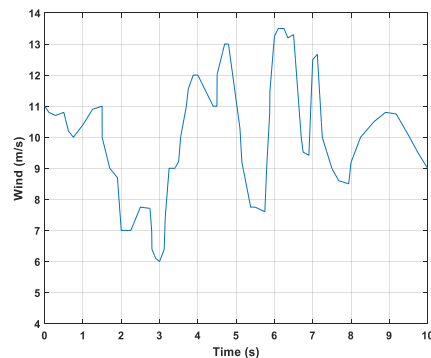


Fig. 19. Second tested wind Speed profile.

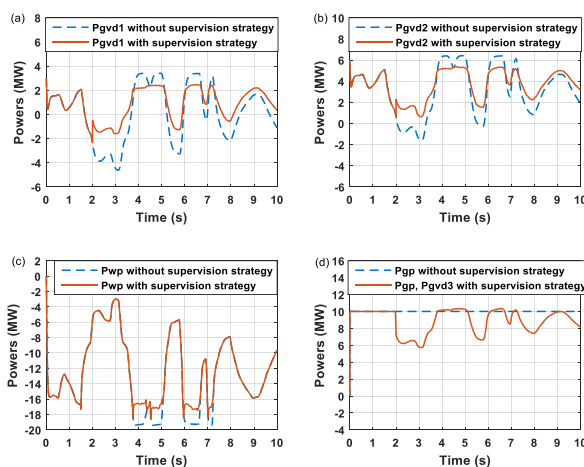


Fig. 20. The evolution of the power in the four terminal HVDC converters without and with the supervision strategy.

At $t=2[s]$, Fig. 20. (a) clearly shows that station 1 reached the limit value of the generated power fixed by the grid code restrictions. In this case, and in order to avoid the risk of damaging the MTDC system and according to the optimisation criteria cited previously, the solution of switching from power to voltage control would be applied and the grid connected power controlled station 4 would become voltage controlled, Fig. 20 (d).

According to Fig. 21, at $t < 2 [s]$, we have 2 power controlled stations and 2 voltage controlled stations, but starting from $t \geq 2 [s]$, the control of the grid station 4 switched from a power controlled station to a voltage controlled one because its contribution to the power generation for the system will be more reliable. Thus, we get an equilibrated MTDC system without reaching the limit value of the generated power fixed by each grid code restriction.

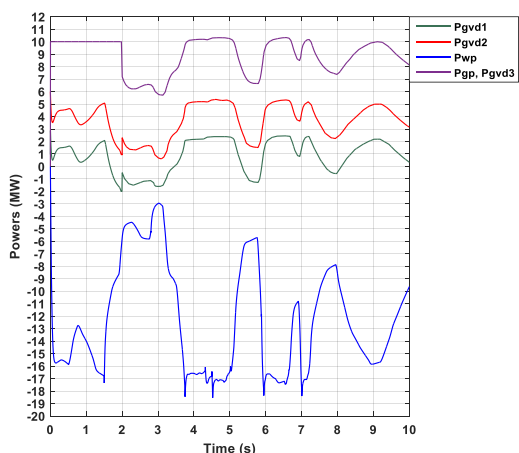


Fig. 21. Power through the four terminal HVDC converters with the supervision strategy. Sections (B) and (C).

Fig. 22 displays the waveform of the DC voltage. We can deduce that after applying sections (B) and (C) of the supervision algorithm, the deviation value of the DC voltage in all the stations of the MTDC system did not exceed 5% in all the time period intervals, which improves the performance sections A, B and C of the algorithm.

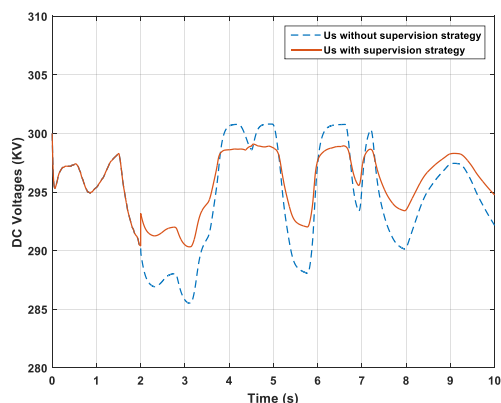


Fig. 22. The MTDC system DC Voltage during implementation of Sections (B) and (C) of the supervision strategy.

- Case of fault occurring in station4 at $t=1s$

From Fig. 21, initially, at $t < 2$ [s], we have 2 power controlled stations and 2 voltage controlled stations. Here, we suppose that at $t = 1s$, a fault occurs on the DC network and converter 4 is lost as shown in Fig. 23 (d). After the occurrence of the fault and even at $t \geq 2$ [s], it is notably clear from Fig. 23 (a) and (b) that both stations 1 and 2 did not reach the limit value of the generated power fixed by each grid code restrictions in all the time intervals. So, there is no need to change the MTDC system initial architecture. This MTDC system still consists of 2 power controlled stations and 2 voltage controlled stations.

Normally, after the application of the fault, stations 1 and 2 which are equipped by voltage droop controllers will help to stabilize the system and compensate the loss of power

which should have been absorbed by converter 4. But, in this case, the grid power reception of stations 1 and 2 exceeded the limits fixed by the grid code restrictions. So, the received power by these voltage droop controlled stations would be set to the maximum value as shown in Fig. 23 (a) and (b) and in order to satisfy the equilibrium of the system, the LPPT was applied for the power generated by the OWF as shown in Fig. 23 (c).

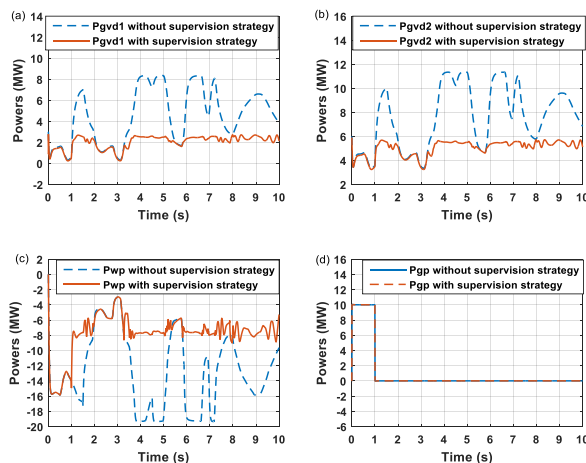


Fig. 23. The power evolution in the four terminal HVDC converters without and with the supervision strategy in case of fault in a power controlled station.

Therefore, it can be deduced from Fig. 24 that even after the application of the fault at $t=1[s]$, the power balance was equilibrated and there was no MTDC station that exceeded the limitation of the generated power fixed by its grid code. So there is no change in the MTDC system initial architecture. Fig. 24 validates the stability of the system and the good performance of sections B and C of the supervision strategy.

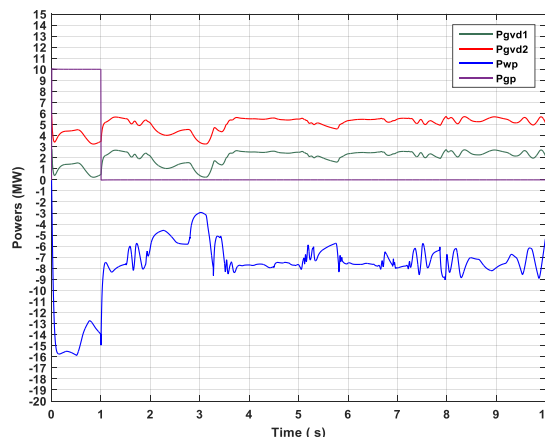


Fig. 24. Power through the four terminal HVDC converters with the supervision strategy in case of fault in a power controlled station.

From Fig. 25, we can deduce that even after the occurrence of the fault in converter 4 of the MTDC system, the deviation value of the DC voltage in all the stations of the MTDC system is still less than 5% at all the time period intervals.

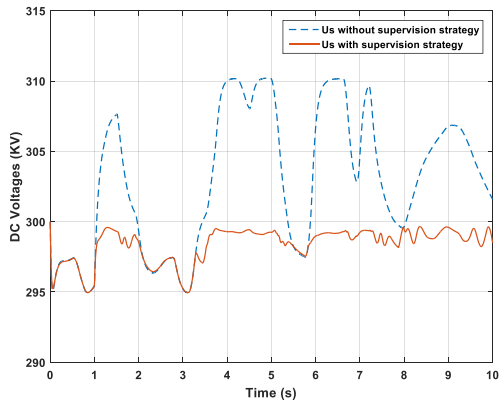


Fig. 25. DC voltages.

- **Case of fault occurring in station 4 at $t=5s$**

As illustrated in Fig. 21, at $t \geq 2$ [s], station 4 switched from a power controlled station to a voltage controlled one. It was supposed that a fault occurred at $t = 5$ [s] in station 4 which is equipped by a voltage droop controller as shown in Fig. 26 (d). So, the others stations which are also equipped by voltage droop controllers should compensate for the fault. However, in this case the grid code limitation of these stations would be not verified and would exceed the maximum value of the received power fixed by the grid code restriction as shown in Fig. 26 (a) and (b). Then, as a solution, we reduced the power generated by the OWF using the LPPT, as shown in Figure 26 (c) in order to set a balance between the power generated and received according to the constraint fixed by the grid code restrictions.

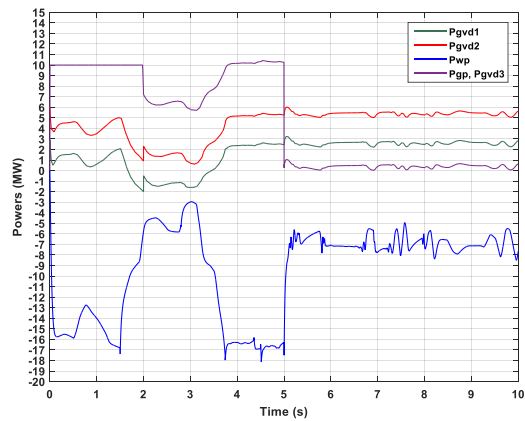


Fig. 27. Power through the four terminal HVDC converters with the supervision strategy in case of fault occurrence in a voltage droop controlled station.

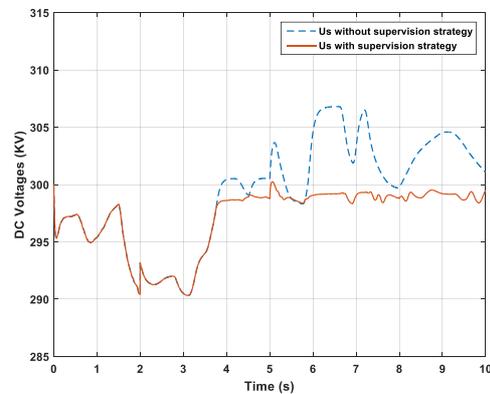


Fig. 28. DC Voltages.

From Fig. 28, it can be deduced that even after the fault occurred in converter 4 of the MTDC system at $t=5$ [s], the deviation value of the DC voltage in all the stations of the MTDC system remained within the specific bounds 5% in all the time period intervals, which shows the effectiveness of Section A of the power management and dedicated control algorithm.

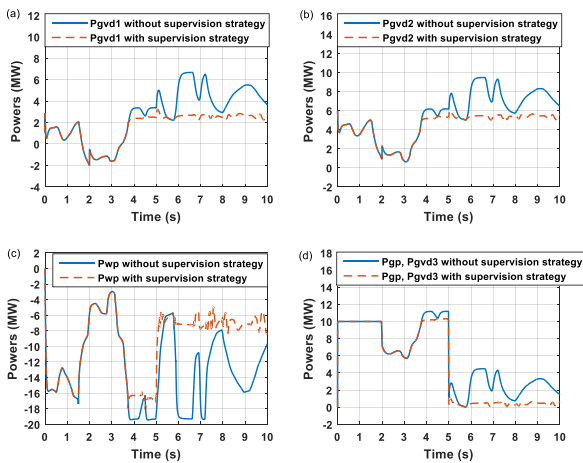


Fig. 26. The evolution of power in the four terminal HVDC converters without and with the supervision strategy in case of fault occurrence in a voltage droop controlled station.

Fig. 27 allows us to note that even after the occurrence of the fault at $t=5$ [s], the power balance was set, the grid code restrictions were verified and the system was stable, which shows the effectiveness of the algorithm.

5. Conclusion

A dynamic decision strategy for energy management of a flexible four terminal VSC-HVDC equipped with a voltage droop control was proposed in this study. The proposed algorithm is composed of three sections A, B and C. Section A is dedicated to the first step control. It serves to choose an adequate droop value, taking into account the DC grid voltage that should remain within specific 5% bounds. In section B, the algorithm was able to define the optimal energy flow management according to the grids constraints in a four terminal VSC-HVDC system equipped with wind farms as a renewable energy production source. In section C, this approach provided the possibility to select the optimum control scheme with some optimization criteria in order to select an optimal architecture based on power flow and dedicated control. In order to design an optimal architecture of the MTDC system with respect to wind speed fluctuations and the different grid code limitations of the stations, our

conceived supervisor takes decisions to choose the suitable procedure by switching the control strategy of a station and acting on the number of connected stations. Then, this approach was generalized to analyze any MTDC system equipped by N stations. The simulation results proved the validity of the proposed power management and control strategy.

Table 1. Studied offshore systems parameters.

Wind Turbine	Value
The wind inertia (J_t)	$30 \cdot 10^6 \text{ kg.m}^2$
Radius (R_t)	60m
λ_{optmal}	8.5
Coefficient (C_{pmax})	0.48
PMSG	Value
Nominal Power	5MW
Stator resistance(R_s)	50mΩ
Self inductance(L_s)	7.5mH
Number of pole pairs(p)	60
Nominal Voltage(U_N)	3300V
Nominal Current (I_N)	933A
inertia of the generator (J_g)	$2 \cdot 10^5 \text{ kg.m}^2$
Nominal torque(T_N)	3380 kN.m

References

[1] Y. E. Abu Eldahab, N. H. Saad, A. Zekry, “Assessing Wind Energy Conversion Systems Based on Newly Developed Wind Turbine Emulator”, International Journal of Smart Grid, Vol.4, No.4, December, 2020.

[2] N. Flourentzou, V. Agelidis and G. Demetriades “VSC-Based HVDC Power Transmission Systems: An Overview”. IEEE Transactions on Power Electronics. Vol. 24. NO. 3, March 2009.

[3] A. F. Guillamon , K. Das, N. A. Cutululis and A. M. Gracia, “Offshore Wind Power Integration into Future Power Systems: Overview and Trends”. Journal of Marin Science and engineering”, 2019.

[4] A. Rekik, G. Boukettaya, R. Kallel, ”Comparative study of two control strategies of a multi-terminal VSC-HVDC Systems”. The 7th International Conference on Systems and Control, Universitat Politècnica de València, Spain, October 24-26, 2018.

[5] A. Harrouz, I. Colak, K. Kayisli, “Control of a small wind turbine system application”, 2016 IEEE International Conference on Renewable Energy Research and Applications (ICRERA).

[6] C. R. Reddy, B. S. Goud;B. N. Reddy;M. Pratyusha;C. V. Kumar;R. Rekha, “Review of Islanding Detection Parameters in Smart Grids”, 2020 8th International Conference on Smart Grid (icSmartGrid).

[7] N. Flourentzou, V. G. Agelidis and G. Demetriades, “Vsc-based hvdc power transmission systems: An overview”. IEEE Transactions on Power Electronics, vol. 24, no.3, pp. 592–602, 2009.

[8] C. Barker and R. Whitehouse “Autonomous converter control in a multi-terminal HVDC system”. 9th IET International Conference on AC and DC Power Transmission, 2010.

[9] H. Teng, L. Ning, Y. Yin, L. Gao,N. Liuand, C. Xie, ”Adaptive Droop Control for DC Voltage Deviation and

Power Sharing in Multi-terminal DC Grids”, ACPEE 2019.

[10] L. Xu and L. Yao. “DC voltage control and power dispatch of a multi-terminal HVDC system for integrating large offshore wind farms”. IET Renewable Power Generation, 5(3):223–233, 2011.

[11] S. Akkari, J. Dai, M. Petit and X. Guillaud, “Interaction between the voltage-droop and the frequency-droop control for multi-terminal HVDC systems”. The Institution of Engineering and Technology, Volume 10, Issue 6, 21 April 2016, p. 1345 – 1352.

[12] S. Sekhar Dash, “Tutorial 1: Opportunities and challenges of integrating renewable energy sources in smart”, 2017 IEEE 6th International Conference on Renewable Energy Research and Applications (ICRERA).

[13] A. Raza, M. Younis , Y. Liu, A. Altalbe , K. Rouzbehi and G. Abbas ,” A Multi-Terminal HVdc Grid Topology Proposal for Offshore Wind Farms”. Applied Sciences, 2020, 10, 1833.

[14] Pedro Rodriguez, Kumars Rouzbehi, “ Multi-terminal DC grids: challenges and prospects”. Journal of Modern Power Systems and Clean Energy volume 5, 2017.

[15] X. Lou, “The Introduction and Analysis of MTDC System”, Proceedings of the 2017. 7th Computer Science Research, July 2017.

[16] R. Torres, A. Graces, G. Diaz, “ HVDC Transmission for Offshore Wind Farms”. Large Scale Renewable Power Generation”. Green Energy and Technology. Springer, 2014, Singapore.

[17] E. Pierri, O. Binder, Naser. G. A. Hemdan, and M. Kurrat. “Challenges and opportunities for a European HVDC grid”. Renewable and Sustainable Energy Reviews, Vol. 70, pp. 427–456, 2017. 37, 43.

[18] E. Veilleux, P. LEHN, “Interconnection of direct-drive wind turbines using DC grid”. 8th International Workshop on Large-Scale Integration of Wind Power into Power Systems as well as on Transmission Networks for Offshore Wind Farms, Bremen, Germany, 2009.

[19] O E. Oni, I E. Davidson, K N .I. Mbangula, “ Areview of LCC-HVDC and VSC-HVDC technologies and applications”. IEEE 16th International Conferenceon Environment and Electrical Engineering, 7-10 June 2016.

[20] M. Khan, M. Iravani, “Hybrid control of a grid-Interactive wind Energy conversion system”. IEEE Transactions on Energy Conversion September 2008.

[21] S. Isik, M. Alharbi , S. Bhattacharya, “ A Feedforward Current Control Strategy for a MMC Based Point to Point HVDCSystems”. 2018 9th IEEE International Symposium on Power Electronics for Distributed Generation Systems, 25-28 June 2018.

[22] C. Dierckxsens, K. Srivastava, M. Reza, S. Cole, J. Beerten and R. Belmans, “A distributed DC voltage control method for VSC MTDC systems”. Elsevier, 2011.

[23] N. Campagna, M. Caruso, V. Castiglia, R. Miceli, F.Viola, “Energy Management Concepts for the Evolution of Smart Grids”, 2020 8th International Conference on Smart Grid (icSmartGrid).